Available online at www.sciencedirect.com
ScienceDirect
Journal of Magnetic Resonance 185 (2007) 308–317
JMR Journal of Magnetic Resonance
www.elsevier.com/locate/jmr

Cross- and axial-peak intensities in 2D-SLF experiments based on cross-polarization—The role of the initial density matrix

Bibhuti B. Das [a], T.G. Ajithkumar [b], Neeraj Sinha [c], Stanley J. Opella [c], K.V. Ramanathan [d,*]

[a] Department of Physics, Indian Institute of Science, Bangalore 560012, India
[b] Central NMR Facility, National Chemical Laboratory, Pune 411008, India
[c] Department of Chemistry and Biochemistry, University of California, San Diego, La Jolla, CA 92093-0307, USA
[d] NMR Research Centre, Indian Institute of Science, Bangalore 560012, India

Received 29 September 2006; revised 8 January 2007
Available online 12 January 2007

Abstract

Simulations and experiments on simple oriented systems have been used to estimate the relative ratio of cross-peak to axial-peak intensities in 2D-SLF experiments based on dipolar oscillations during cross-polarization (CP). The density matrix prior to dipolar evolution is considered and for an isolated spin pair, it is shown that direct calculations of the ratios match well with simulations and experimental results. Along with the standard CP pulse sequence, two other pulse sequences namely CP with polarization inversion (PI–CP) and another novel variation of the standard CP experiment (EXE-CP) reported recently have been considered. Inclusion of homonuclear dipolar coupling has been observed to increase the axial-peak intensities. In combination with Lee–Goldburg (LG) decoupling, experiments on an oriented liquid crystalline sample have been carried out and the performance of the pulse schemes have been compared. The applicability of the new pulse sequence for different samples and different nuclei is discussed. Such studies are expected to lead to a better understanding of the experiments and to the design of useful pulse sequences.
© 2007 Elsevier Inc. All rights reserved.

Keywords: SLF; Oriented molecules; PISEMA; Cross polarization

1. Introduction

Measurement of heteronuclear dipolar couplings by the use of dipolar oscillations observed during cross-polarization [1] incorporated into 2D-SLF experiments [2] has become one of the important methods of structural elucidation of oriented molecules. Both nematic liquid crystals, which orient in a magnetic field and membrane peptides and proteins, which are aligned either by magnetic fields or by macroscopic means have been extensively studied by this technique [3–7]. In this method spin evolution during polarization transfer gives rise to the dipolar cross-peaks, which for a two spin system can be understood to arise from evolution under mutually commuting zero- and double-quantum sub-spaces [8]. Under conditions of exact Hartmann–Hahn match, the evolution in the zero-quantum sub-space alone contributes to the dipolar cross-peak while the evolution in the double-quantum sub-space contributes only to the axial-peak. Increasing the cross-peak intensity enhances the sensitivity of the experiment, while suppression of the axial-peak enables resolution of cross-peaks arising from small dipolar couplings. This requires that the initial density matrix is essentially of zero-quantum in nature which can, for example, be achieved by polarization inversion (PI) [9]. Subsequently, the dipolar oscillations are monitored with the removal of the homonuclear dipolar couplings by a suitable decoupling scheme. An example of such a combination of the above two features is the PISEMA experiment [10].

* Corresponding author. Fax: +91 80 23601550.
E-mail address: KVR@SIF.IISC.ERNET.IN (K.V. Ramanathan).

1090-7807/$ - see front matter © 2007 Elsevier Inc. All rights reserved.
doi:10.1016/j.jmr.2007.01.007

Thus the protocol for the design of these class of experiments consists of two parts namely the preparation of the initial density matrix prior to the t_1 evolution and the pulse sequence during the dipolar evolution during the t_1 period. The latter part of such experiments, where the actual polarization transfer through heteronuclear dipolar couplings takes place while homonuclear dipolar couplings are removed has received considerable attention. Several pulse sequences that are aimed at aspects such as better homonuclear decoupling efficiency and reduced sample heating and off-set effects have been proposed [11–17]. Detailed descriptions of the procedure to be adapted for setting up of such experiments are also available [18]. However very little attention has been paid to the initial preparation of the density matrix. Polarization inversion prior to dipolar evolution is generally accepted as the standard protocol. Though PI was known for a long time and has been used in a number of situations [19–26] to the best of our knowledge there are very few studies in the context of the measurement of dipolar coupling through the SLF experiments [9]. There have also been very few reports of investigation of alternate methods of preparation of the initial density matrix [27].

In this article we present quantitative comparison of the relative ratio of cross-peak to axial-peak intensities in three different experiments. Two of these are the standard Hartmann–Hahn cross-polarization (CP) and the polarization inversion cross-polarization (PI–CP) experiments. The third one is a modified CP experiment in which an initial 90° pulse on the X-nucleus is added to the standard H–H cross-polarization and involves the equilibrium magnetization of the X-nucleus in the CP process [27]. These three experiments differ in the preparation of the initial density matrix. During the subsequent evolution period one may use any of the heteronuclear polarization transfer protocols based on spin exchange combined with a suitable homonuclear decoupling sequence such as the FSLG sequence used in PISEMA [10] and its variants [11–15] or the sequence used in SAMMY [16,17]. In this presentation we have used either LG or FSLG decoupling wherever necessary. We present results of simulation carried out using SIMPSON [28] and experimental results on oriented ^{13}C labeled chloroform and dichloromethane samples. A discussion of the effects of homonuclear coupling on the spectrum is also presented. Application of these pulse sequences to the nematic liquid crystal 4-*n*-pentyl-4′-cyanobiphenyl (5CB) and to a single crystal of [15] labeled *N*-acetyl leucine, provides comparisons in terms of practical utility of the sequences.

2. Theory

We begin by considering the equilibrium magnetization of both the *I* and *S* spins and then analyze how they contribute to the magnetization in the zero- and the double-quantum sub-spaces that determine the relative ratio of the cross-peak to axial-peak intensities. Fig. 1 presents two dipolar coupled spins *I* and *S* with equilibrium populations of the respective α and β states being N^I_α, N^I_β and N^S_α, N^S_β. We assume that the *I* and *S* spins have equal abundance. For natural abundance Carbon-13 or Nitrogen-15 this would amount to considering only those protons (*I* spins) having a ^{13}C or ^{15}N (*S* spins) as a coupled partner. We then have,

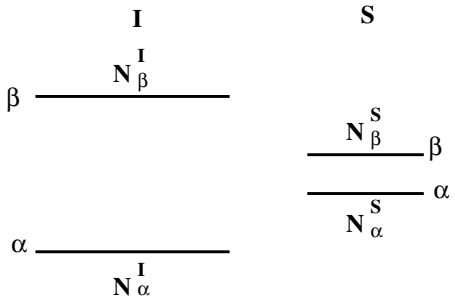

Fig. 1. Equilibrium populations for two dipolar coupled *I* and *S* spins.

$$N^I_\alpha + N^I_\beta = N^S_\alpha + N^S_\beta = N \tag{1}$$

Let

$$N^I_\alpha - N^I_\beta = n_I \text{ and } N^S_\alpha - N^S_\beta = n_S \tag{2}$$

In equilibrium and under high temperature approximation, let

$$\frac{n_S}{n_I} \approx \frac{\gamma_S}{\gamma_I} = k \tag{3}$$

We can divide this population distribution into sub-populations of the double- and zero-quantum states as,

Double-quantum :

$$N_{\alpha\alpha} = N^I_\alpha \times \frac{N^S_\alpha}{N} \text{ and } N_{\beta\beta} = N^I_\beta \times \frac{N^S_\beta}{N} \tag{4}$$

Zero-quantum :

$$N_{\alpha\beta} = N^I_\alpha \times \frac{N^S_\beta}{N} \text{ and } N_{\beta\alpha} = N^I_\beta \times \frac{N^S_\alpha}{N} \tag{5}$$

Here, $\frac{N^S_\alpha}{N}$ represents the fraction of *S* spins in state α and $\frac{N^S_\beta}{N}$ represents the fraction in state β, such that

$$N_{\alpha\alpha} + N_{\alpha\beta} = N^I_\alpha \times \frac{N^S_\alpha + N^S_\beta}{N} = N^I_\alpha \tag{6}$$

Similarly,

$$N_{\beta\alpha} + N_{\beta\beta} = N^I_\beta, \quad N_{\alpha\alpha} + N_{\beta\alpha} = N^S_\alpha, \quad N_{\alpha\beta} + N_{\beta\beta} = N^S_\beta \tag{7}$$

The double- and zero-quantum magnetizations given by $M_Z{}^\Sigma$ and $M_Z{}^\Delta$ are proportional to $(N_{\alpha\alpha} - N_{\beta\beta})$ and $(N_{\alpha\beta} - N_{\beta\alpha})$, respectively.

Leaving out the proportionality constants, we write,

$$M_Z^{\Delta} = N_{\alpha\beta} - N_{\beta\alpha} = \frac{N_\alpha^I N_\beta^S - N_\beta^I N_\alpha^S}{N}, \tag{8}$$

$$M_Z^{\Sigma} = N_{\alpha\alpha} - N_{\beta\beta} = \frac{N_\alpha^I N_\alpha^S - N_\beta^I N_\beta^S}{N} \tag{9}$$

$$\begin{aligned} M_Z^{\Sigma} + M_Z^{\Delta} &= \frac{1}{N}\left[N_\alpha^I(N_\alpha^S + N_\beta^S) - N_\beta^I(N_\alpha^S + N_\beta^S)\right] \\ &= N_\alpha^I - N_\beta^I = M_I \end{aligned} \tag{10}$$

Similarly,

$$M_Z^{\Sigma} - M_Z^{\Delta} = N_\alpha^S - N_\beta^S = M_S \tag{11}$$

Here, M_I and M_S are the magnetizations corresponding to I and S spins, respectively. From Eqs. (8) and (9), the ratio of cross-peak intensity arising from zero-quantum magnetization to the axial-peak intensity arising from double-quantum magnetization is obtained as,

$$R_{\mathrm{ZQDQ}} = \frac{1}{2}\frac{N_\alpha^I N_\beta^S - N_\beta^I N_\alpha^S}{N_\alpha^I N_\alpha^S - N_\beta^I N_\beta^S} \tag{12}$$

where the factor $\frac{1}{2}$ has been introduced since in the 2D-SLF experiment, the cosine modulation of the ZQ magnetization gives rise to two cross-peaks in the F_1 dimension. The above expression can be used to estimate the relative ratio of cross-peak to axial-peak intensities for three different cross-polarization pulse schemes shown in Fig. 2.

2.1. Standard CP

Fig. 2a is the standard cross-polarization sequence. In this scheme, the equilibrium proton I-spin polarization evolves during t_1, giving rise to the dipolar oscillations monitored during t_2 with S spin signal. The dipolar oscillation is visualized by considering the I_Z magnetization in the tilted rotating frame as a double-quantum (DQ) density matrix $\frac{1}{2}(I_Z + S_Z)$ and a zero-quantum (ZQ) density matrix $\frac{1}{2}(I_Z - S_Z)$ [8]. Under exact Hartmann–Hahn match and high rf power, the DQ density matrix remains essentially unaltered, giving rise to the axial-peak in the 2D spectrum and the ZQ term oscillates as $\frac{1}{2}(I_Z - S_Z)\cos(\mathrm{d}t_1)$, where d is the dipolar coupling. Together they give an S spin evolution given by $\frac{1}{2}S_Z(1 - \cos(\mathrm{d}t_1))$. The Fourier transform then yields the dipolar peaks in the F_1 dimension. The relative intensities of the cross-peak to the axial-peak depends on the ratio of the ZQ population difference to the DQ population difference as represented by $(N_{\alpha\beta} - N_{\beta\alpha})$ and $(N_{\alpha\alpha} - N_{\beta\beta})$, respectively. In this case the initial 90° pulse is only on the I spin, in contrast to the pulse scheme shown in Fig. 2b. Hence the polarization of the S spin in the B_0 magnetic field is not used and in the tilted rotating frame the α and β states of S are equally populated. Therefore $N_\alpha^S = N_\beta^S = \frac{N}{2}$. Hence from Eqs. (8) and (9),

$$N_{\alpha\beta} - N_{\beta\alpha} = N_{\alpha\alpha} - N_{\beta\beta} = \frac{N_\alpha^I - N_\beta^I}{2} \tag{13}$$

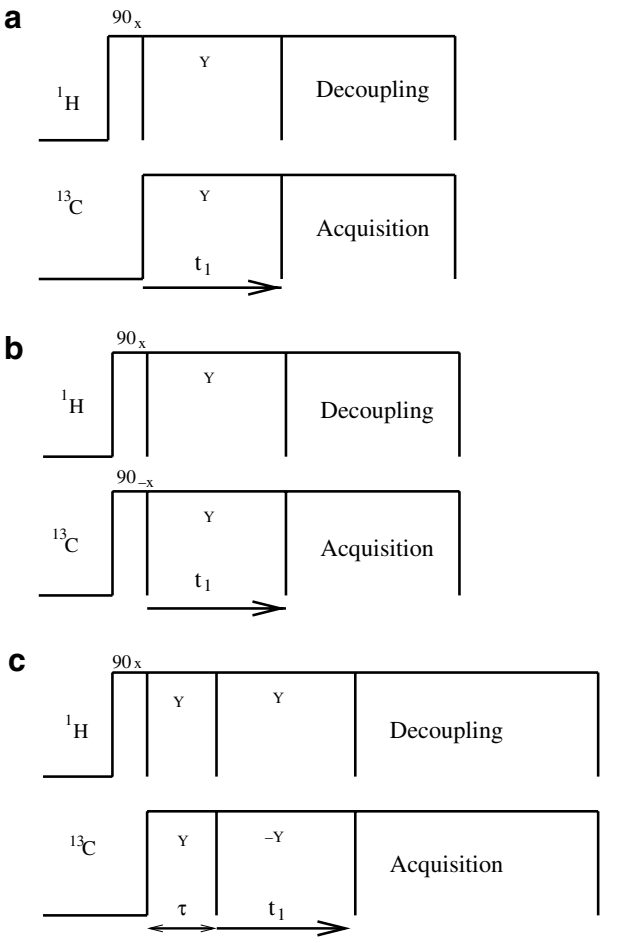

Fig. 2. (a) Conventional CP pulse sequence with dipolar evolution during t_1 period. (b) EXE-CP pulse sequence which includes an additional 90° pulse on carbon (S spin) in the CP sequence. The phase of the pulse is opposite to that of the 90° pulse on proton (I spin) (c) PI–CP pulse sequence with an initial cross-polarization period τ to achieve exclusively initial ZQ density matrix at the start of t_1 period.

Therefore, the cross-peak has half of the axial-peak intensity and $R_{\mathrm{ZQDQ}} = 0.5$.

2.2. Equilibrium X-nuclear-polarization enhanced cross-polarization (EXE-CP)

Fig. 2b is a modification to the standard CP pulse sequence wherein an initial 90° pulse is added to the S spin also [27]. This introduces the equilibrium S magnetization in the cross-polarization process. However, the phase of the 90° pulse is such that the combined density matrix in the tilted rotating frame enhances the zero-quantum part of the density matrix in comparison to the double-quantum part, as described below.

Using Eqs. (1)–(3),

$$N_\alpha^S + N_\beta^S = N$$
$$N_\alpha^S - N_\beta^S = k(N_\alpha^I - N_\beta^I)$$

we get,

$$N_\alpha^S = \frac{N + k(N_\alpha^I - N_\beta^I)}{2} \tag{14}$$

$$N_\beta^S = \frac{N - k(N_\alpha^I - N_\beta^I)}{2} \tag{15}$$

In Fig. 2b, because the S spin is polarized in a sense opposite to that of the I spins during the spin-lock period, the labels α and β get interchanged for the S spin. So Eqs. (14) and (15) are modified as,

$$N_\alpha^S = \frac{N - k(N_\alpha^I - N_\beta^I)}{2} \tag{16}$$

$$N_\beta^S = \frac{N + k(N_\alpha^I - N_\beta^I)}{2} \tag{17}$$

Substituting the above in Eqs. (8) and (9),

$$\begin{aligned} M_Z^\Delta &= \frac{1}{N}(N_\alpha^I N_\beta^S - N_\beta^I N_\alpha^S) \\ &= \frac{1}{2}(N_\alpha^I - N_\beta^I)(1+k) \\ M_Z^\Sigma &= \frac{1}{N}(N_\alpha^I N_\alpha^S - N_\beta^I N_\beta^S) \\ &= \frac{1}{2}(N_\alpha^I - N_\beta^I)(1-k) \end{aligned}$$

$$R_{\mathrm{ZQDQ}} = \frac{1}{2}\frac{1+k}{1-k} \tag{18}$$

For carbon with $k \approx \frac{1}{4}$, $R_{\mathrm{ZQDQ}} = 0.83$.

In other words, the cross-peak intensity in a 2D-SLF experiment increases by 25%. whereas, the axial-peak intensity goes down by the same amount resulting in a 67% relative enhancement of cross-peak to axial-peak. That this produces perceptible and desirable effect on the 2D-SLF spectrum is illustrated in the experimental section.

2.3. Cross-polarization with polarization inversion (PI–CP)

Fig. 2c includes an initial ^{13}C polarization period τ, during which the proton bath consisting of the rest of the protons polarize the two spins I and S such that the S spin population matches that of the I spin. Therefore at the end of the polarization period (τ) and at the beginning of the polarization inversion period (t_1), when the labels α and β of the S spin are interchanged, the populations are given by,

$$N_\alpha^I = N_\beta^S \text{ and } N_\beta^I = N_\alpha^S$$

From Eqs. (8) and (9), the DQ and ZQ magnetizations are given by,

$$M_Z^\Sigma = 0 \text{ and } M_Z^\Delta = \frac{1}{N}[(N_I^\alpha)^2 - (N_I^\beta)^2)] = N_I^\alpha - N_I^\beta \tag{19}$$

Comparing Eqs. (19) and (13), there is a twofold increase in the intensity of the ZQ magnetization, whereas the initial DQ magnetization is zero. This should result in the complete absence of the axial-peak with R_{ZQDQ} tending to a very large number. In practice, there are other factors that contribute to the axial-peak, such as the presence of homonuclear couplings among protons. In the subsequent section we present experimental results and simulations that confirm the above observations.

3. Experimental

Experiments have been carried out on an oriented sample of ^{13}C labeled chloroform oriented in the liquid crystal *N*-(*p*′-ethoxybenzylidine)-*p*-*n*-butylaniline (EBBA) at room temperature on a Bruker DSX-300 FTNMR spectrometer with a proton resonance frequency of 300.13 MHz and a ^{13}C resonance frequency of 75.47 MHz, using a double resonance MAS probe without spinning the sample. The carbon spectrum of this sample shown in Fig. 3a is a doublet with a separation of 7.72 kHz equal to $J + 2D$, where J is the indirect spin–spin couplings and D is the dipolar

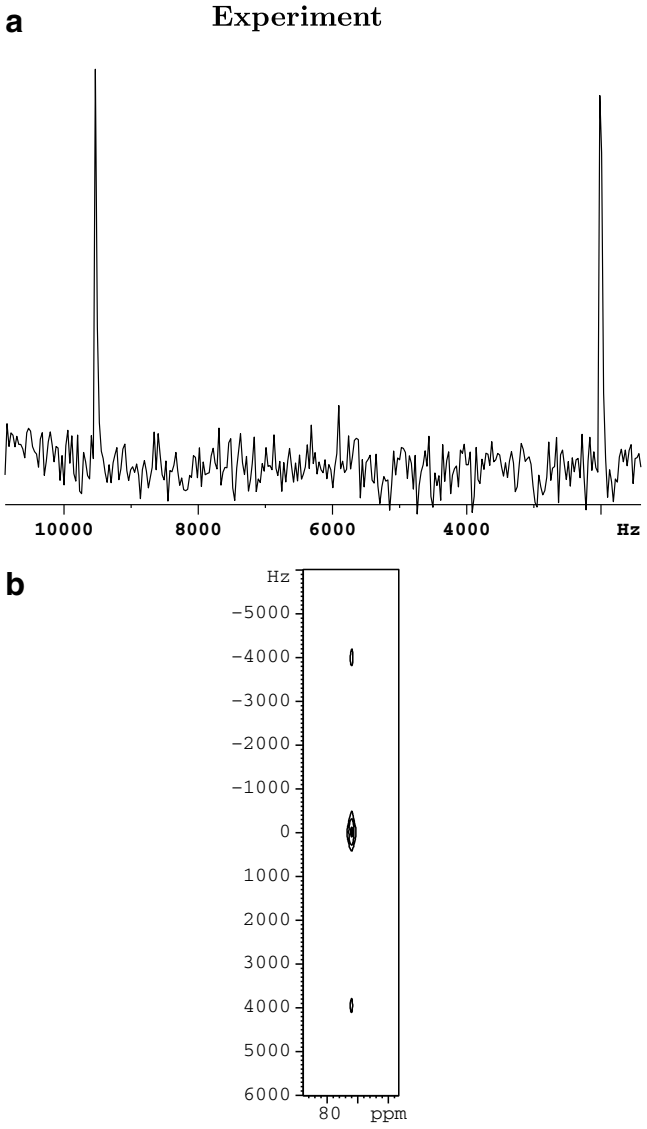

Fig. 3. (a) Proton coupled ^{13}C spectrum of ^{13}C labeled chloroform oriented in the liquid crystal EBBA. (b) 2D-SLF spectrum of chloroform obtained using the CP pulse scheme shown in Fig. 2a.

coupling between proton and carbon scaled by the order parameter along the C–H vector [29]. This sample serves as a model isolated I–S spin pair. We have also carried out experiments on ^{13}C labeled dichloromethane ($^{13}CH_2Cl_2$) (DCM) oriented in the liquid crystal EBBA. In this case the protons have equal coupling to the carbon and also have a dipolar coupling between themselves and the spin-system serves as an isolated I_2S system. The 2D-SLF pulse scheme shown in Figs. 2a–c have been employed to record the spectra of the oriented chloroform sample while the pulse schemes of Figs. 2a and b have been applied on the oriented DCM sample. Experiments have also been carried out on an oriented sample of the nematic liquid crystal 5CB at room temperature. In this case the pulse sequences have been modified to include homo-nuclear dipolar decoupling during the t_1 period using the LG sequence with spin exchange at the magic angle [10]. Typically the 2D data were acquired with 64 t_1 increments of 65 μs each. Recycle delay of 15 s was used to avoid sample heating. 30 kHz rf was used for both proton and carbon during cross-polarization and 55 kHz rf was used for proton decoupling. t_1 domain data were zero filled to 512 points and the data set of 4096×512 were double Fourier transformed in magnitude mode. An experimental 2D-SLF spectrum of chloroform obtained using Fig. 2a is shown in Fig. 3b. In subsequent discussion the cross-section through the contours is discussed. In order to check the performance of the different pulse sequences for nuclei with very low gyromagnetic ratio, similar experiments involving ^{15}N have also been carried out on an ^{15}N labeled single crystal sample of N-acetyl leucine (NAL) on a Varian UNITY INOVA NMR spectrometer at a proton operating frequency of 500 MHz.

4. Results and discussion

Figs. 4a–c show simulation results of the 2D-SLF experiments obtained using the programme SIMPSON [28] for two heteronuclear spins corresponding to the pulse schemes shown in Fig. 2. Fig. 4a is the F_1 cross-section corresponding to the experiment that utilizes the standard CP evolution as depicted in Fig. 2a, in which the initial density matrix is I_Z. Evolution of the spin-locked magnetization during t_1 gives rise to both cross-peaks and axial-peaks corresponding to evolution in the zero- and double-quantum sub-spaces, respectively. Each of the cross-peak has half the intensity of the axial-peak as expected based on Eq. (13). Fig. 4b corresponds to an initial density matrix $I_Z + \frac{\gamma_S}{\gamma_I} S_Z$, but with the pulse phases adjusted such that the I and S magnetizations are polarized in the opposite directions during spin-lock such that the density matrix becomes $I_Z - \frac{\gamma_S}{\gamma_I} S_Z$ in the tilted rotating frame. This gives rise to an additional contribution to the zero-quantum density matrix and the subsequent evolution enhances the intensity for the cross-peak while reducing the axial-peak intensity. For $\frac{\gamma_S}{\gamma_I} = 0.25$, this gives the intensity ratio predicted by Eq. (18). The EXE-CP pulse scheme of Fig. 2b achieves this, as this utilizes the equilibrium magnetization of both I and S spins. The two $\pi/2$ pulses on both I and S and spin-lock in opposite directions give rise to a higher

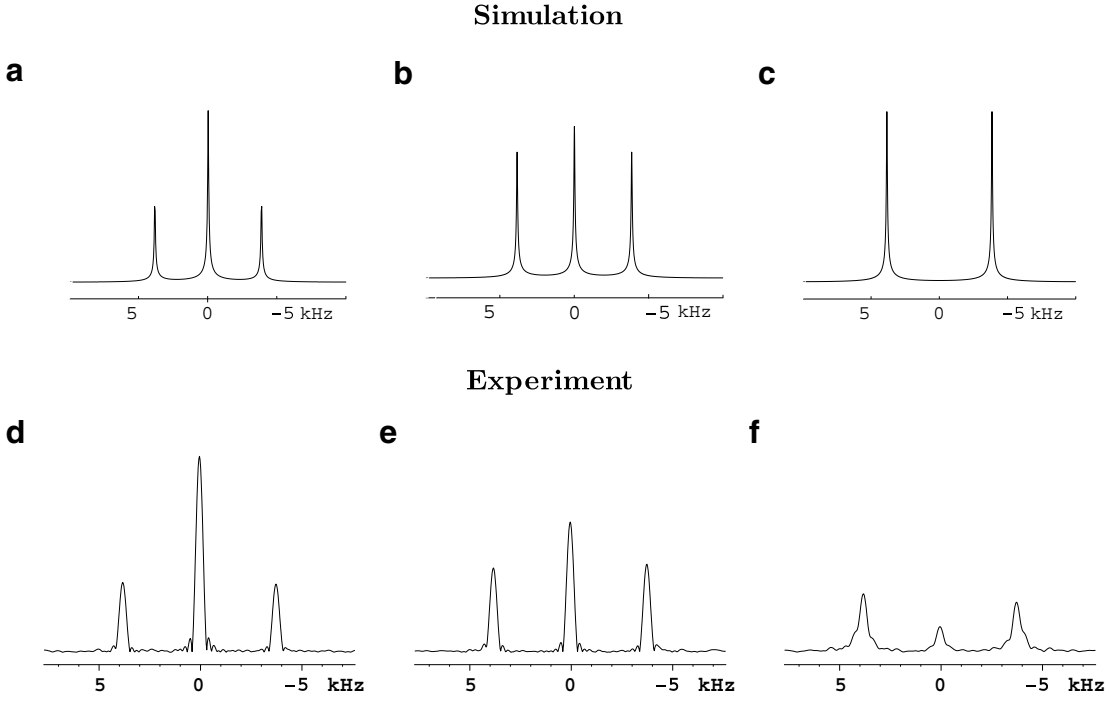

Fig. 4. (a–c) Simulation results obtained corresponding to pulse sequences of Figs. 2a–c, respectively. For b and c, $\frac{\gamma_S}{\gamma_I}$ have been taken to be $\frac{1}{4}$ and 1, respectively (vide text for details) (d–f). F_1 cross-sections of 2D-SLF spectrum of chloroform acquired using the pulse sequences shown in Figs. 2a–c, respectively.

contribution to the zero-quantum part of the density matrix and to the cross-peaks as detailed in the theory section.

Fig. 4c corresponds to the initial density matrix equal to $I_Z - S_Z$ which corresponds to equal polarization but with opposite phases for the I and S spins. In hetero-nuclear cases it is achieved by an initial polarization period in which the S spins attain a population differences equal to the I spins and a subsequent inversion of the polarization of the S spins. Such a process is achieved by the PI–CP pulse-scheme shown in Fig. 2c. Experimental demonstration of the results is described below.

Figs. 4d and e show cross-sections through the 2D-SLF spectrum for spectra recorded with the standard CP sequence of Fig. 2a and the modified EXE-CP sequence of Fig. 2b, respectively. In Fig. 4d it is observed that the axial-peak dominates the spectrum, while in Fig. 4e its intensity is considerably reduced and the cross-peak intensity is enhanced. The ratio R_{ZQDQ} is 0.36 and 0.65 for the two experiments. This is slightly lower than the values of 0.5 and 0.83 expected based on Eqs. (13) and (18) and arises because even small mismatch of the Hartmann–Hahn condition increases the axial-peak intensity as seen in simulation and in experiments (results not shown). Results obtained for the PI–CP experiment of Fig. 2c are shown in Fig. 4f. In this case, the initial polarization at the beginning of the t_1 period is in the ZQ subspace, which is achieved for oriented chloroform as follows [30]. The initial polarization period τ is adjusted to be equal to $\frac{1}{4d}$, where d is the proton carbon dipolar coupling obtained from the spectrum of Fig. 3a. During this period the zero-quantum component evolves into unobservable magnetization components [8], while the double-quantum component remains unchanged. The subsequent inversion of one of the rf field directions at the beginning of the t_1 period, converts the DQ magnetization to ZQ magnetization. As a result, the axial-peak arising from time development in the DQ subspace is very nearly absent. Thus the results of simulation and experiment shown in Fig. 4 agree well with those expected based on considerations of relative populations of the spin states. They also demonstrate the usefulness of utilizing the equilibrium population difference of the X-nucleus.

Chloroform provides an ideal isolated heteronuclear two spin system. But in other samples with more protons present, the homonuclear dipolar couplings (D_{HH}) between protons provide additional polarization pathways that increase the non-oscillatory magnetization component. Hence, even with polarization inversion an axial-peak of non-negligible intensity appears in the spectrum. This is illustrated in Fig. 5. Figs. 5a–c present spectra simulated for dichloromethane (DCM) corresponding to the CP experiment. They have been obtained for different values of homonuclear couplings viz. 0, 5 and 8 kHz, respectively, while the heteronuclear coupling between the carbon and the protons is retained at 5 kHz. It is observed that the presence of homonuclear dipolar coupling results in the increase in the intensity of axial-peaks. This happens even with the inclusion of S nuclear polarization as seen in simulation results shown in Figs. 5d–f, but the increase is less for smaller values of (D_{HH}). This is also seen in the experiments with DCM. Fig. 5g shows the spectrum obtained using the CP experiment while Fig. 5h, recorded using the EXE-CP pulse scheme shows a significant reduction of the axial-peak intensity. Inclusion of homonuclear couplings have other effects on the spectra as well. For example, the cross-peaks have split into two lines in the spectra shown in Figs. 5g and h. This is also observed in the simulated spectra shown in Figs. 5b, c, e and f.

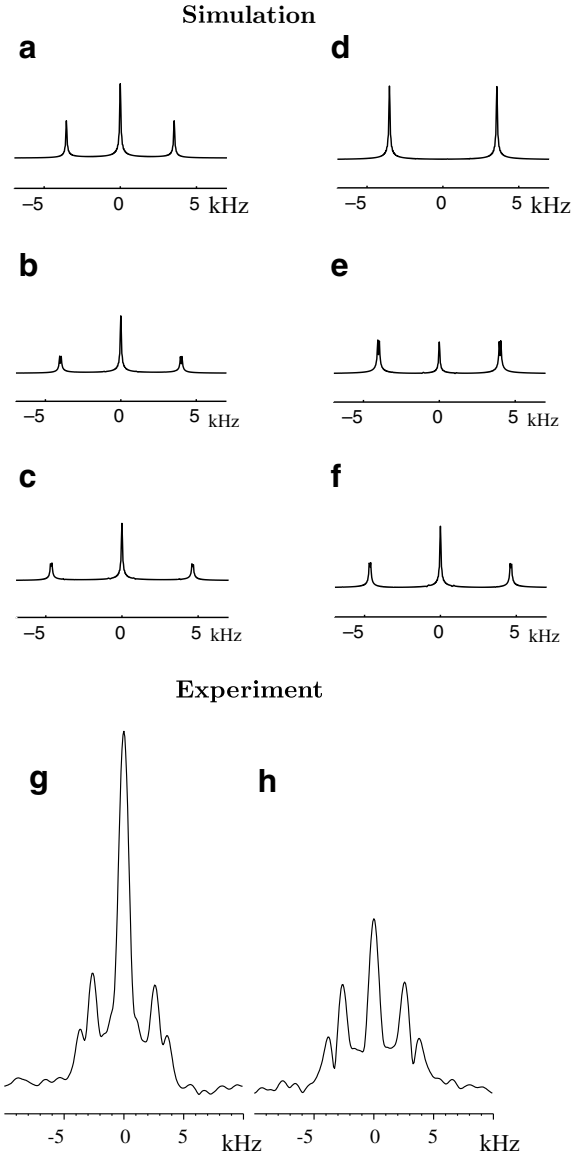

Fig. 5. (a–f) Simulation results for an I_2S spin system (a–c) correspond to the initial density matrix being I_Z and (d–f) correspond to the initial density matrix being $I_Z - S_Z$. The hetero nuclear dipolar coupling d_{IS} is 5 kHz for all the cases. The homonuclear dipolar coupling d_{II} is 0 kHz (a and d), 5 kHz (b and e), 8 kHz (c and f). (g and h) F_1 cross-sections of 2D-SLF spectrum of DCM obtained using the pulse sequence shown in Figs. 2a and b.

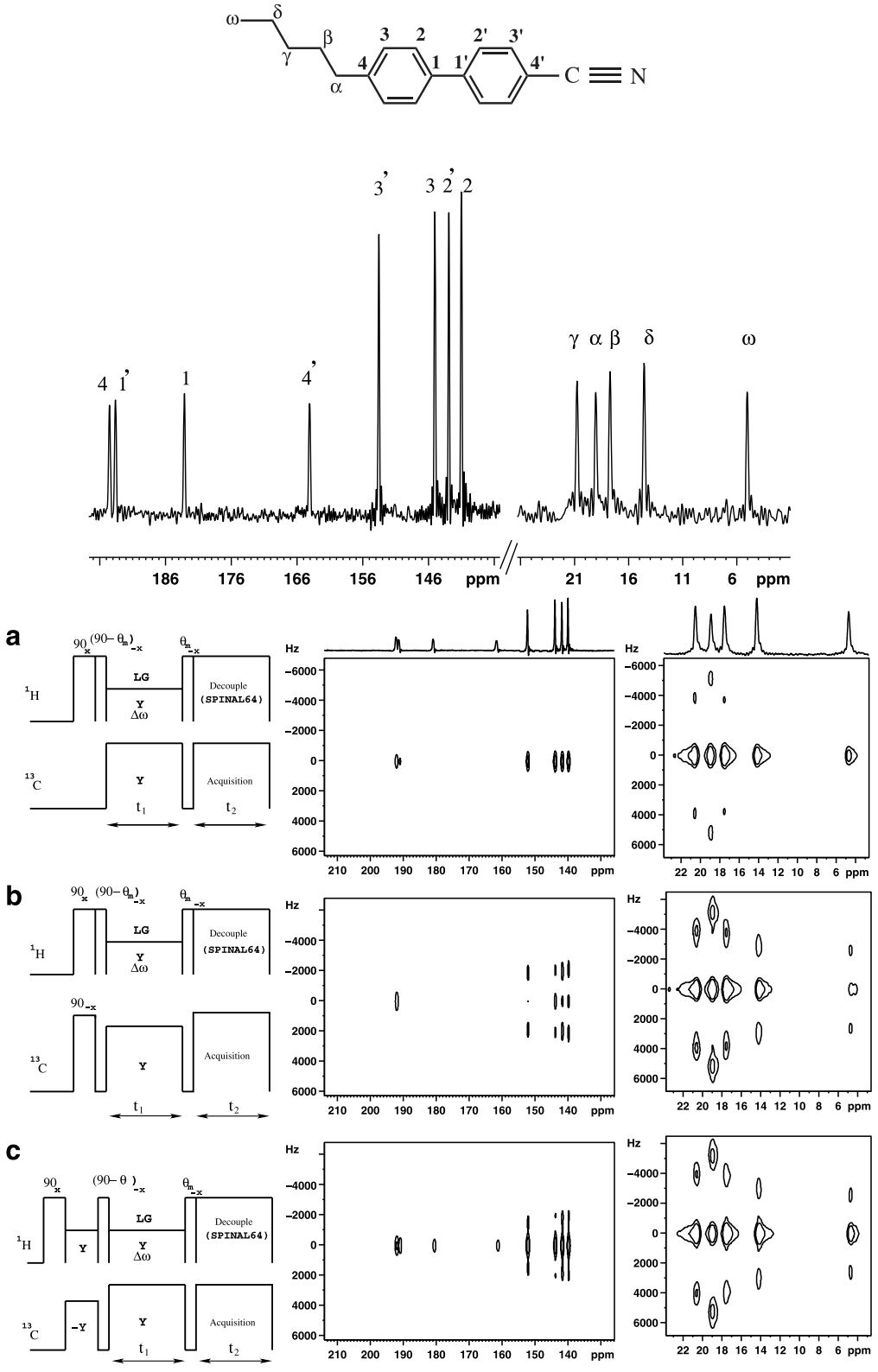

Fig. 6. (a) LGCP (b) EXE-LGCP and (c) PI-LGCP pulse sequences obtained from Figs. 2a, b and c modified to include a LG sequence for homonuclear decoupling during t_1 period. Experimental results obtained on a sample of the liquid crystal 5CB are shown in each case. Molecular structure and the 1D proton decoupled ^{13}C spectrum of the liquid crystal are shown at the top. Aliphatic and aromatic regions of the spectra are shown separately both in the 1D and 2D-spectra. In the 2D-spectra, the horizontal axis corresponds to the carbon chemical shift in ppm scale and the vertical axis corresponds to the proton-carbon dipolar coupling in kHz.

In order to study the performance of the three pulse schemes in the case of a more complex system, experiments have been carried out on an oriented sample of the nematic liquid crystal 5CB. In this case the strong homonuclear dipolar couplings among protons dominate the spectra and need to be eliminated in order to observe the dipolar oscillations and the effect of the different initial density matrices for the spin exchange process. This is achieved by including Lee–Goldburg decoupling together with polarization transfer at the magic angle [10,31] for each of the pulse sequences as shown in Fig. 6. The corresponding 2D spectra obtained are also shown in the same figure. It is observed that cross-peak intensities obtained with the LGCP pulse scheme of Fig. 6a are very much less than those obtained with pulse schemes of Figs. 6b and c. Cross-sections corresponding to several carbons in 5CB obtained with the three pulse sequences are presented in Fig. 7. In the figure, it may be noticed that the relative cross-peak intensities obtained with the EXE-LGCP pulse scheme of Fig. 6b is either equal to or higher than those obtained with the PI-LGCP sequence shown in Fig. 6c. This is contrary to expectation, but the result can be understood as follows. At the end of the polarization inversion period, if the initial density matrix is of entirely zero-quantum in nature i.e. of the type, $I_Z - S_Z$, then the axial-peak will have the least intensity. On the other hand, if the contact time during PI is short and the S spins are not fully polarized, then the resulting density matrix will be of the form, $I_Z - p{\cdot}S_Z$, where p is less than one. Dipolar oscillations during PI can also result in p less than 1. In these

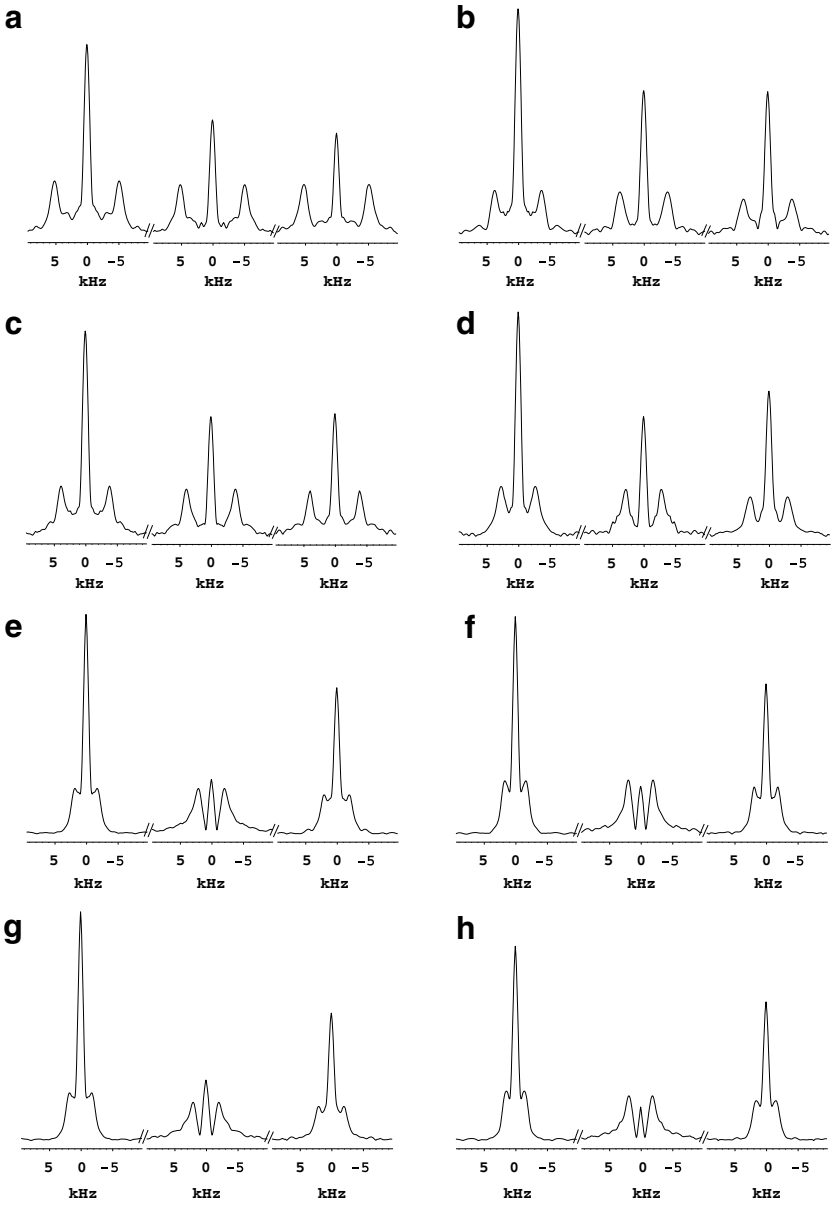

Fig. 7. F_1 cross-sections of the 2D-SLF spectra of 5CB shown in Fig. 6 for different carbons: (a) α (b) β (c) γ (d) δ (e) 2 (f) 2′ (g) 3 (h) 3′ carbons. Columns one, two and three correspond to spectra obtained with the pulse sequences shown in Figs. 6a, b and c, respectively.

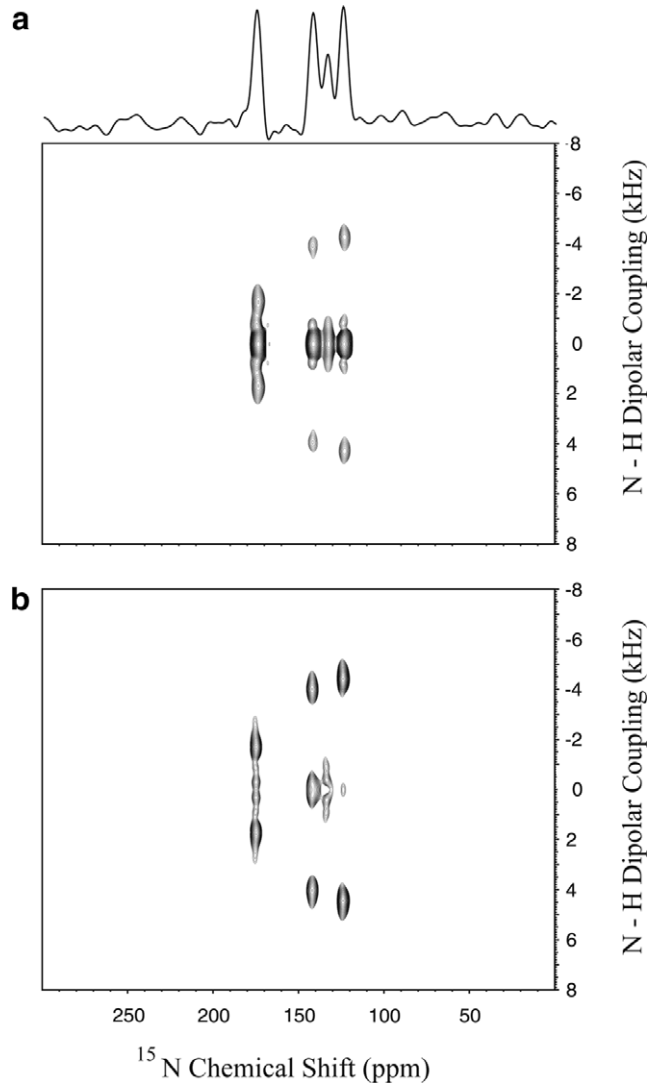

Fig. 8. ^{1}H–^{15}N 2D-SLF spectra of a single crystal of ^{15}N labeled *N*-acetyl leucine obtained using (a) EXE-SEMA and (b) PISEMA pulse sequences. There are four molecules in the unit cell which give rise to four different ^{15}N resonances with different ^{1}H–^{15}N dipolar couplings.

cases the axial-peak intensity will be higher and the performance of the experiment with PI is degraded. Earlier experiments with PI on the same sample report a better axial-peak suppression [13,14], where a longer contact time of 4 ms has been used [14] in comparison to 1 ms used here. Thus, EXE-LGCP seems to perform better than PI-LGCP when the polarization inversion time is short. Since rf irradiation used during the preparation period in the case of EXE-LGCP is negligible this could offer an advantage over polarization inversion based methods in terms of lower sample heating. Further refinement of the pulse schemes, where frequency switched LG (FSLG) decoupling replaces the LG decoupling in the t_1 period in Fig. 6c leads to the well-known PISEMA scheme. A similar modification on Fig. 6b may be called EXE-SEMA. Implementation of these experiments on 5CB gave results similar to those depicted in Figs. 6 and 7. It may be mentioned that since the EXE-CP experiment uses the direct polarization available from the B_0 field for both the nuclei, it is necessary that the relaxation time of the nuclei involved is short. In the case of liquid crystals, the ^{13}C relaxation time was estimated to be of the order of a few hundreds of milliseconds and hence the new pulse scheme is found to be effective. We have also carried out the EXE-SEMA experiment for the case of a very low γ nucleus such as ^{15}N by implementing it on a sample of ^{15}N labeled *N*-acetyl leucine. In this case the direct polarization available from the B_0 field for the X-nucleus is small and hence its contribution to the zero-quantum magnetization is also small which will result in a higher axial-peak intensity. This is observed to be so as illustrated in Fig. 8 which also shows the PISEMA spectrum for comparison. The PISEMA spectrum (Fig. 8b) is found to provide a higher cross-peak intensity than EXE-SEMA spectrum (Fig. 8a).

5. Conclusions

2D-SLF experiments based on dipolar oscillations during cross-polarization constitute an important class of experiments for structure and dynamics studies of oriented biological and liquid crystalline systems. In order to estimate the relative ratio of cross-peak to axial-peak intensities in these experiments simulation and simple oriented systems have been used. In this presentation we have utilized ^{13}C labeled chloroform to study dipolar oscillations in oriented static samples. Quantitative estimates of the contribution from the initial density matrix prior to t_1 evolution to the cross- and axial-peaks for an isolated heteronuclear spin pair have been obtained for three different experiments. These agree well with spectra obtained by simulation and with experiments. Additionally, the role of homonuclear dipolar coupling has been studied by considering a simple system of two equivalent I spins coupled to an S spin. It is shown that homonuclear dipolar couplings contribute to increasing the axial-peak intensity at the expense of cross-peaks, emphasizing the usefulness of homonuclear dipolar decoupling sequences. The new pulse sequence EXE-CP, proposed recently and which employs a pair of 90° pulses with opposite phases on I and S spins prior to t_1 evolution and the PI–CP sequence have been further investigated in combination with homonuclear dipolar decoupling sequences. The new sequence would be useful, where it is essential to reduce the rf energy input into the sample during the initial preparation period. However, the applicability of the scheme which utilizes X-nucleus polarization in the B_0 field is limited by the following two factors namely, (i) the relaxation time of the X-nucleus which will determine the repetition rate between scans and the duration of the experiment and (ii) the gyromagnetic ratio of the X-nucleus—the ones with a smaller value will have very little direct polarization available. These aspects have been illustrated with studies on different systems using two different heteronuclei.

Acknowledgments

The use of the DSX-300 NMR spectrometer funded by the Department of Science and Technology(DST), New Delhi at the NMR Research Centre, Indian Institute of Science, Bangalore is gratefully acknowledged.This research also utilized the Biomedical Technology Resource for NMR Molecular Imaging of Proteins at the University of California, San Diego supported by Grant P41EB002031 from the National Institutes of Health.

References

[1] L. Muller, A. Kumar, T. Baumann, R.R. Ernst, Transient oscillations in NMR cross-polarization experiments in solids, Phys. Rev. Lett. 32 (1974) 1402.
[2] R.K. Hester, J.L. Ackerman, V.R. Cross, J.S. Waugh, Resolved dipolar coupling spectra of dilute nuclear spins in solids, Phys. Rev. Lett. 34 (1975) 993.
[3] K.V. Ramanathan, Neeraj Sinha, in: N. Muller, P.K. Madhu (Eds.), Current Developments in Solid State NMR Spectroscopy, vol. III, Springer Verlag, Wien, 2003.
[4] T. Narasimhaswamy, D.K. Lee, N. Somanathan, A. Ramamoorthy, Solid-state NMR characterization of a novel thiophene-based three phenyl ring mesogen, Chem. Mater. 17 (2005) 4567.
[5] T. Narasimhaswamy, M. Monette, D.K. Lee, N. Somanathan, A. Ramamoorthy, Solid-state NMR characterization and determination of the orientational order of a Nematogen, J. Phys. Chem. B 109 (2005) 19696.
[6] F.M. Marassi, A. Ramamoorthy, S.J. Opella, Complete resolution of the solid-state NMR spectrum of a uniformly ^{15}N-labeled membrane protein in phospholipid bilayers, Proc. Natl. Acad. Sci. USA 94 (1997) 8551.
[7] J. Wang, J. Denmy, C. Tian, S. Kim, Y. Mo, F. Kovacs, Z. Song, K. Nishimura, Z. Gan, R. Fu, J.R. Quine, T.A. Cross, Imaging membrane protein helical wheels, J. Magn. Reson. 144 (2000) 162.
[8] M.H. Levitt, D. Sutar, R.R. Ernst, Spin dynamics and thermodynamics in solid-state NMR cross polarization, J. Chem. Phys. 84 (1986) 4243.
[9] Neeraj Sinha, K.V. Ramanathan, Use of polarization inversion for resolution of small dipolar couplings in SLF-2D NMR experiments – an application to liquid crystals, Chem. Phys. Lett. 332 (2000) 125.
[10] C.H. Wu, A. Ramamoorthy, S.J. Opella, High-resolution heteronuclear dipolar solid-state NMR spectroscopy, J. Magn. Reson. A109 (1994) 270.
[11] D.K. Lee, T. Narasimhaswamy, A. Ramamoorthy, PITANSEMA, a low-power PISEMA solid-state NMR experiment, Chem. Phys. Lett. 399 (2004) 359.
[12] K. Yamamoto, D.K. Lee, A. Ramamoorthy, Broadband-PISEMA solid-state NMR spectroscopy, Chem. Phys. Lett. 407 (2005) 289.
[13] K. Nishimura, A. Naito, Dramatic reduction of the rf power for attenuation of sample heating in 2D-separated local field solid-state NMR spectroscopy, Chem. Phys. Lett. 402 (2005) 245.
[14] S.V. Dvinskikh, D. Sandstrom, Frequency offset refocused PISEMA-type sequences, J. Magn. Reson. 175 (2005) 163.
[15] K. Nishimura, A. Naito, Remarkable reduction of rf power by ATANSEMA and DATANSEMA separated local field in solid-state NMR spectroscopy, Chem. Phys. Lett. 419 (2006) 120.
[16] A.A. Nevzorov, S.J. Opella, A magic sandwich pulse sequence with reduced offset dependence for high-resolution separated local field spectroscopy, J. Magn. Reson. 164 (2003) 182.
[17] A.A. Nevzorov, S.J. Opella, Selective averaging for high-resolution solid-state NMR spectroscopy of aligned samples, J. Magn. Reson. (2006), doi:10.1016/j.jmr.2006.09.006.
[18] A. Ramamoorthy, C.H. Wu, S.J. Opella, Experimental aspects of multidimensional solid-state NMR correlation spectroscopy, J. Magn. Reson. 140 (1999) 131.
[19] N. Zumbulyadis, 1H/29Si cross-polarization dynamics in amorphous hydrogenated silicon, J. Chem. Phys. 86 (1987) 1162.
[20] D.G. Cory, Separation of non-protonated from protonated carbon NMR resonances in solids by inversion-recovery cross-polarization, Chem. Phys. Lett. 152 (1988) 431.
[21] X. Wu, S. Zhang, X. Wu, Selective polarization inversion in solid state high-resolution CP MAS NMR, J. Magn. Reson. 77 (1988) 343.
[22] X.L. Wu, K.W. Zilm, Complete spectral editing in CPMAS NMR, J. Magn. Reson. A102 (1993) 205.
[23] R. Sangill, N.R. Anderson, H. Bildose, H.J. Jacobsen, N.C. Nielsen, Optimized spectral editing of 13C MAS NMR Spectra of rigid solids using cross-polarization methods, J. Magn. Reson. A107 (1994) 67.
[24] P. Tekely, F. Montigny, D. Canet, J.J. Delpuech, High-resolution dipolar NMR spectra in rotating solids from depolarization of the rare spin magnetization, Chem. Phys. Lett. 175 (1990) 401.
[25] P. Palmas, P. Tekely, D. Canet, Local-field measurements on powder samples from polarization inversion of the rare-spin magnetization, J. Magn. Reson. A104 (1993) 26.
[26] P. Reinheimer, J. Hirschinger, P. Gilard, N. Goetz, Cross-polarization dynamics and proton dipolar local field measurements in some organic compounds, Magn. Reson. Chem. 35 (1997) 757.
[27] Bibhuti B. Das, T.G. Ajithkumar, K.V. Ramanathan, Enhancing cross-peak intensity in 2D-SLF spectroscopy – the role of equilibrium carbon magnetization in cross-polarization experiments, Chem. Phys. Lett. 426 (2006) 422.
[28] M. Bak, J.T. Rasmussen, N.C. Nielsen, SIMPSON: a general simulation program for solid-state NMR spectroscopy, J. Magn. Reson. 147 (2000) 296.
[29] P. Diehl, C.L. KhetrapalNMR-basic Principles and Progress, vol. 1, Springer-Verlag, Heidelberg, 1969, p. 1.
[30] Neeraj Sinha, Ph. D. thesis, Indian Institute of Science, Bangalore, India, 2003.
[31] C.S. Nagaraja, K.V. Ramanathan, Determination of order parameters of liquid crystals: use of dipolar oscillations enhanced by Lee–Goldburg decoupling, Liq. Cryst. 26 (1999) 17.